

Electronic Supplementary Information for Desorption Dynamics of CO₂ from Formate Decomposition on Cu(111)

Fahdzi Muttaqien,^{*,†} Hiroyuki Oshima,[†] Yuji Hamamoto,^{†,‡} Kouji Inagaki,^{†,‡}
Ikutaro Hamada,[†] and Yoshitada Morikawa^{*,†,‡,¶}

[†]*Department of Precision Science and Technology, Graduate School of Engineering, Osaka
University, 2-1, Yamada-oka, Suita, Osaka 565-0871, Japan*

[‡]*Elements Strategy Initiative for Catalysts and Batteries (ESICB), Kyoto University,
Katsura, Kyoto 615-8520, Japan*

[¶]*Research Center for Ultra-Precision Science and Technology, Graduate School of
Engineering, Osaka University, Japan*

E-mail: fahdzi@cp.prec.eng.osaka-u.ac.jp; morikawa@prec.eng.osaka-u.ac.jp

S1 – Calculation methods

The calculations were performed using the STATE code, which previously has been used for formate adsorption,¹ formate hydrogenation,² CO₂ hydrogenation,³ CO₂ dissociation,⁴ and *ab initio* molecular dynamics (AIMD) study of methanol electrooxidation.⁵ As mentioned in the main text, we compared the results obtained using the Perdew-Burke-Ernzerhof (PBE)⁶ functional with those using several vdW density functionals (vdW-DFs), i.e., the original vdW-DF (vdW-DF1),^{7,8} optB86b-vdW,⁹ and rev-vdW-DF2¹⁰ functionals. We also included the dispersion correction proposed by Grimme with PBE (PBE-D2).¹¹ The implementation of the self-consistent vdW-DF¹²⁻¹⁴ in the STATE code is described in Ref. 15. The cut-off energies of 36 and 400 Ry were used for the wave functions and the augmented charge density, respectively. The electron-ion interaction was described using Vanderbilt’s ultrasoft pseudopotentials.¹⁶ The Cu(111) surface was modeled using a three layer-thick (3×3) unit cell with the bottommost atomic layer fixed to its bulk configuration. The distance between the two neighboring slabs is more than 30 Å. We sampled the surface Brillouin zone using a uniform grid of $4 \times 4 \times 1$ k -points. We used the climbing image nudged elastic band (CI-NEB) method^{17,18} to obtain the minimum energy path, the transition state (TS), and the activation energies of formate synthesis from CO₂ hydrogenation. We calculated the vibrational frequencies of the adsorbed species at the TS using the frozen phonon approximation. We obtained one imaginary frequency in the TS structure, which indicated that the geometry was a first-order saddle point on the potential energy curve. Starting from the TS structure, we performed AIMD simulations to evaluate the translational and internal (rotational and vibrational) energies of desorbed CO₂ from the Cu surface. The detailed description of the TS structures are shown in Fig. S1 and Table S1. In these simulations, the initial velocities are given randomly and they are scaled to make the average kinetic energy of 300 K. Here, we do not include zero-point energy in the sampling of initial conditions. The system was evolved without velocity scaling or thermostat.

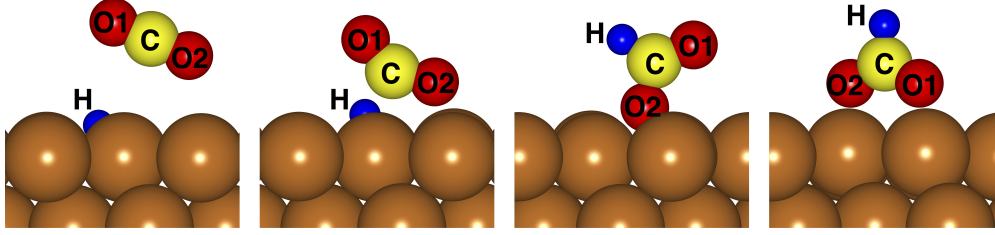


Figure S 1: From left to right panel: configuration of initial state (IS), transition state (TS), monodentate formate (mo-HCOO), and bidentate formate (bi-HCOO) structures, respectively. The red, yellow, blue, and brown circles represent oxygen, carbon, hydrogen, and Cu atoms, respectively.

Table S 1: Detailed descriptions of the structures depicted in Fig. S1. The bond length (C–O1, C–O2, and C–H) and bond distance (Cu–O2 and Cu–H), and bond angle are in Å and degree, respectively.

	PBE	PBE-D2	vdW-DF1	rev-vdW-DF2	optB86b-vdW
Initial state					
C–O1	1.18	1.18	1.18	1.18	1.18
C–O2	1.18	1.18	1.18	1.18	1.18
C–H	2.97	2.98	3.12	2.90	2.91
Cu–O2	3.30	2.98	3.21	2.90	2.92
Cu–H	0.88	0.87	0.85	0.89	0.88
$\angle_{\text{O1-C-O2}}$	179.81	179.60	179.93	179.84	179.82
Transition state					
C–O1	1.20	1.20	1.20	1.20	1.20
C–O2	1.23	1.24	1.24	1.25	1.24
C–H	1.58	1.49	1.49	1.51	1.48
Cu–O2	2.17	2.13	2.23	2.06	2.13
Cu–H	1.35	1.31	1.25	1.31	1.20
$\angle_{\text{O1-C-O2}}$	147.04	144.27	144.83	143.36	144.59
Monodentate formate					
C–O1	1.22	1.22	1.22	1.22	1.22
C–O2	1.35	1.35	1.36	1.36	1.36
C–H	1.11	1.11	1.11	1.11	1.11
Cu–O2	1.40	1.39	1.41	1.40	1.40
Cu–H	3.35	3.34	3.36	3.36	3.34
$\angle_{\text{O1-C-O2}}$	124.27	124.07	124.13	123.92	123.92
Bidentate formate					
C–O1	1.27	1.27	1.28	1.27	1.27
C–O2	1.27	1.27	1.28	1.27	1.27
C–H	1.11	1.11	1.10	1.11	1.11
Cu–O2	2.02	2.01	2.05	2.01	2.01
Cu–H	3.67	3.68	3.75	3.73	3.75
$\angle_{\text{O1-C-O2}}$	127.82	127.56	127.63	127.46	127.49

S2 – AIMD trajectories

As we mentioned in the main text, we have also considered additional samples of the initial geometry for AIMD simulations. The additional geometries were derived from the original TS geometry (shown in Table S1) by slightly moving the atoms within a hyperplane perpendicular to the reaction coordinate. In this procedure, we moved the atoms towards the second, third, fourth, fifth, and sixth lowest normal mode vectors from the TS, which were obtained from the vibrational frequency analysis. The displacement was done so that the new initial geometry has 0.02 eV energy different with the original initial geometry. The additional calculations were done using one of vdW-fucntionals (optB86b-vdW). Based on our calculations (shown in the Table S2), the average results from several samples of AIMD trajectory indicate that most of formate synthesis energy is transferred into bending mode of CO₂.

Table S 2: Calculated translational energy (E_t), rotational energy (E_r), vibrational energy of bending mode (E_b), and vibrational energy of symmetric stretching mode (E_s) of desorbed CO₂ from formate decomposition on Cu(111) calculated using optB86b-vdW functional (in eV). The AIMD simulations were done starting from different initial geometries that were derived from the original TS geometries by slightly moving the atoms within a hyperplane perpendicular to the reaction coordinate.

	First	Second	Third	Fourth	Fifth	Sixth	Average
E_t	0.11	0.14	0.16	0.12	0.18	0.11	0.14 ^a
E_r	0.10	0.09	0.11	0.09	0.17	0.07	0.11
E_b	0.25	0.27	0.24	0.26	0.22	0.30	0.26
E_s	0.07	0.02	0.03	0.05	0.01	0.03	0.04
Surf. mode ^b	0.02	0.03	0.01	0.03	0.07	0.04	0.03

^aThe calculated CO₂ translational energy as a formate decomposition product is in good agreement with experimentally reported results in Ref. 19.

^bThis energy is deduced from the following: $E_a(\text{syn}) - (E_t + E_r + E_b + E_s)$.

S3 – Evaluation of CO₂ translational and internal energies

We estimated the CO₂ translational energy (E_t) from the velocity of the center of mass of CO₂ (v_{COM}):

$$E_t = \frac{1}{2} m_{\text{CO}_2} \sum v_{\text{COM}}^2 \quad (1)$$

The rotational energy (E_r) of CO₂ was estimated from the moment of inertia of CO₂ (I) and its angular momentum (L) at each time step of the AIMD trajectory:

$$E_r = \frac{1}{2} \sum L_i I_{ij}^{-1} L_j \quad (2)$$

Meanwhile, the energy of each CO₂ vibrational mode is evaluated from the time evolution of the desorbed CO₂ geometry. We gathered the geometry data of desorbed CO₂, i.e., bond angle (θ), the C–O bond length (l), and the difference between two C–O bond lengths (Δ), which represent the bending, symmetric, and antisymmetric stretching modes of CO₂, respectively, when the desorbed CO₂ has already had constant translational energy. We then determined the amplitude and period of these geometry changes. Next, based on these amplitude data, we estimated the energy of each vibrational mode of desorbed CO₂ by fitting them into the database of the relative stability of isolated CO₂ as a function of the θ , l , and Δ (shown in Fig. S2). For an example, the amplitude of the CO₂ bond angle in one period is between 160.6° and 199.4° as shown in the top panel of Fig. 3. If we fit this value to the data for the relative stability of isolated CO₂, it shows that desorbed CO₂ has a bending mode energy of approximately 0.25 eV.

The calculated vibrational frequencies of isolated CO₂ molecule are shown in the Table S3.

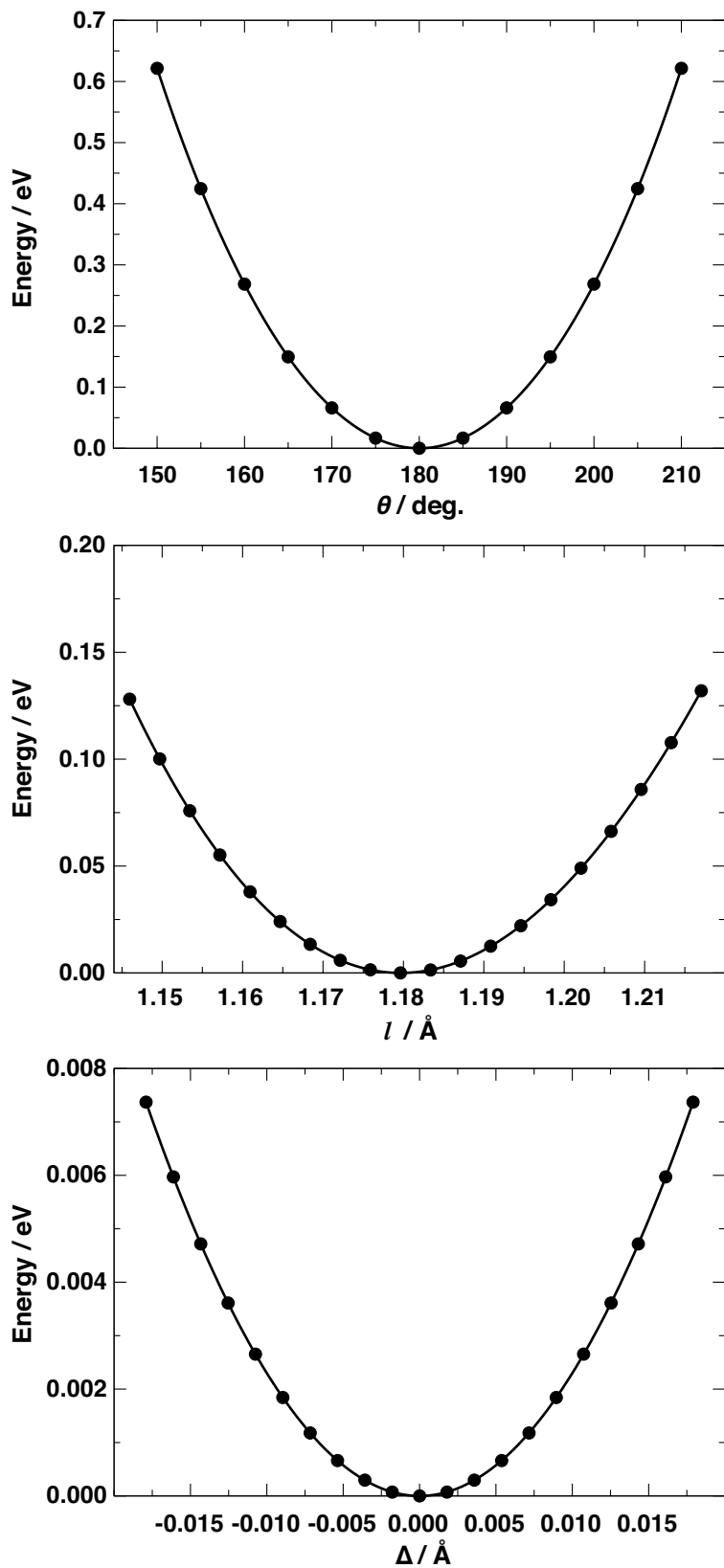


Figure S 2: Relative stability of an isolated CO₂ molecule with respect to its bond angle (θ), the C–O bond length (l), and the difference between two C–O bond lengths (Δ).

Table S 3: Calculated vibrational frequencies of bending (ν_b), symmetric stretching (ν_s), antisymmetric stretching (ν_{as}) modes, and C–O bond length (l) of isolated CO₂ using PBE, PBE-D2, and vdW-DFs. The frequency and bond length are in meV and Å, respectively.

	This study					Expt.
	PBE	PBE-D2	vdW-DF1	rev-vdW-DF2	optB86b-vdW	
ν_b	77.34	77.59	76.19	76.58	76.72	82.70 ^a
ν_s	164.91	164.47	162.78	164.48	164.61	165.27 ^b
ν_{as}	296.83	296.11	291.38	295.14	295.74	291.24 ^b
l	1.179	1.180	1.182	1.179	1.179	1.162 ^c

^aTaken from Ref. 20.

^bTaken from Ref. 21.

^cTaken from Ref. 22.

S4 – Sudden Vector Projection Analysis

We performed the sudden vector projection (SVP) analysis, which was proposed by Jiang and Guo,^{23–25} to determine which desorbed CO₂ modes are excited during the decomposition process. Based on the SVP analysis (shown in the Table S4), the CO₂ bending mode has second larger projection value compare with its translational, symmetric and antisymmetric stretching modes. It indicates that the bending mode of desorbed CO₂ is excited during the decomposition process. Therefore, this result is agree with our molecular dynamics analysis.

Table S 4: Comparison of the projection values of the translational and vibrational modes of CO₂ and H atom onto the CO₂ hydrogenation reaction modes at TS.

	SVP value
CO ₂ -translation	0.12
CO ₂ -bending	0.27
CO ₂ -symmetric	0.04
CO ₂ -antisymmetric	0.02
H-translation	0.79

The SVP analysis also shows that the kinetic mode of adsorbed hydrogen has the largest projection value. The large projection value of kinetic mode of hydrogen atom might be due to its displacement with respect to the surface. Hydrogen atom is easier to move since it has smaller mass compare with CO₂ molecule. However, this may not indicate that

excitation of adsorbed hydrogen will enhance formate synthesis. It is because we obtained quite small portion of transferred energy into the surface mode as shown in the Table 2 in the main manuscript. Therefore, we think that the molecular dynamics analysis is necessary to elucidate the excited modes of desorbed CO₂.

References

- (1) Morikawa, Y.; Iwata, K.; Nakamura, J.; Fujitani, T.; Terakura, K. *Chem. Phys. Lett.* **1999**, *304*, 91–97.
- (2) Morikawa, Y.; Iwata, K.; Terakura, K. *Appl. Surf. Sci.* **2001**, *169-170*, 11–15.
- (3) Wang, G.; Morikawa, Y.; Matsumoto, T.; Nakamura, J. *J. Phys. Chem. B* **2006**, *110*, 9–11.
- (4) Muttaqien, F.; Hamamoto, Y.; Inagaki, K.; Morikawa, Y. *J. Chem. Phys.* **2014**, *141*, 034702.
- (5) Herron, J. A.; Morikawa, Y.; Mavrikakis, M. *P. Natl. Acad. Sci. USA* **2016**, *113*, E4937–E4945.
- (6) Perdew, J. P.; Burke, K.; Ernzerhof, M. *Phys. Rev. Lett.* **1996**, *77*, 3865–3868.
- (7) Dion, M.; Rydberg, H.; Schröder, E.; Langreth, D. C.; Lundqvist, B. I. *Phys. Rev. Lett.* **2004**, *92*, 246401.
- (8) Dion, M.; Rydberg, H.; Schröder, E.; Langreth, D. C.; Lundqvist, B. I. *Phys. Rev. Lett.* **2005**, *95*, 109902.
- (9) Klimeš, J.; Bowler, D. R.; Michaelides, A. *Phys. Rev. B* **2011**, *83*, 195131.
- (10) Hamada, I. *Phys. Rev. B* **2014**, *89*, 121103.
- (11) Grimme, S. *J. Comput. Chem.* **2006**, *27*, 1787–1799.
- (12) Thonhauser, T.; Cooper, V. R.; Li, S.; Puzder, A.; Hyldgaard, P.; Langreth, D. C. *Phys. Rev. B* **2007**, *76*, 125112.
- (13) Román-Pérez, G.; Soler, J. M. *Phys. Rev. Lett.* **2009**, *103*, 096102.
- (14) Wu, J.; Gygi, F. *J. Chem. Phys.* **2012**, *136*, 224107.

- (15) Hamamoto, Y.; Hamada, I.; Inagaki, K.; Morikawa, Y. *Phys. Rev. B* **2016**, *93*, 245440.
- (16) Vanderbilt, D. *Phys. Rev. B* **1990**, *41*, 7892–7895.
- (17) Mills, G.; Jónsson, H.; Schenter, G. K. *Surf. Sci.* **1995**, *324*, 305–337.
- (18) Henkelman, G.; Uberuaga, B. P.; Jónsson, H. *J. Chem. Phys.* **2000**, *113*, 9901–9904.
- (19) Quan, J.; Kondo, T.; Wang, G.; Nakamura, J. *Angew. Chem. Int. Edit.* **2017**, *56*, 3496–3500.
- (20) Person, W. B.; Zerbi, G. *Vibrational intensities in infrared and Raman spectroscopy*; Elsevier Scientific Pub. Co.: Amsterdam, Netherland, 1982.
- (21) Shimanouchi, T. *Tables of Molecular Vibrational Frequencies, Consolidated Volume 1*; National Standard Reference Data System (NSRDS): Tokyo, Japan, 1972.
- (22) Herzberg, G. *Electronic Spectra and Electronic Structure of Polyatomic Molecules*; D. Van Nostrand Co., Inc.: Princeton, New Jersey, 1966.
- (23) Jiang, B.; Guo, H. *J. Chem. Phys.* **2013**, *138*, 234104.
- (24) Guo, H.; Jiang, B. *Acc. Chem. Res.* **2014**, *47*, 3679–3685, PMID: 25393632.
- (25) Jiang, B.; Yang, M.; Xie, D.; Guo, H. *Chem. Soc. Rev.* **2016**, *45*, 3621–3640.

Graphical TOC Entry

